J. Fluid Mech. (1996), vol. 327, pp. 117–138

Mechanics of collisional motion of granular materials. Part 4. Expansion wave

By A. GOLDSHTEIN, M. SHAPIRO† AND C. GUTFINGER
Faculty of Mechanical Engineering, Technion-Israel Institute of Technology, Haifa 32000, Israel

(Received 1 March 1995 and in revised form 5 November 1995)

The problem of expansion into a vacuum of a semi-infinite layer composed of chaotically moving inelastic rough spherical particles is solved analytically. A variant of the matched asymptotic expansion scheme is used to obtain a matched composite solution, which is valid for both small and large times in the wave head, wave tail and intermediate domains of the disturbed part of the layer.

The effects of granular initial energy and particle collisonal properties on their hydrodynamic velocity, temperature, density and pressure are studied in the limit of low initial density of the granular gas. The total granular mass, M, within the disturbed region was found to change with time as $\log t$. This is in contrast with the comparable classical result $M \sim t$ obtained for conservative (molecular) gases. This logarithmic dependence stems from the influence of kinetic energy losses, which reduce the granular temperature and speed of sound in the wave head region.

The ultimate escape energy and momentum (i.e. those achieved for long times by the expanding part of the layer) are shown to be finite quantities, dependent on the particle restitution coefficient, roughness and the initial granular temperature. The estimated mass of the escaping part of the layer, calculated here for dilute gases, serves as an upper bound on this quantity for all (also dense) comparable granular gases. This mass is determined by the collisional losses, as embodied within the particle restitution and roughness coefficients.

1. Introduction

Granular materials are frequently met in Nature and various industrial, geological and environmental applications. Products of modern chemical, food, pharmaceutical and agricultural industries often come in the form of grains or powders. Modelling of moving powder and granular materials is thus an important problem in various technological processes. Although people have long been using these materials (e.g. sand), the cumulative behaviour of moving grains is still not well understood. They may either move like solids or exhibit a complicated rheological liquid-like behaviour.

The physical principles governing the motion of granular materials depend upon the interparticle forces. The motion of densely packed granules is governed mainly by the Coulomb frictional forces. On the other hand, collisional motion is affected by the particle impacts. In several cases (e.g. in shear-induced motion) both types of motion may take place simultaneously. When modelling granular flows, domains where each type prevails, as well as the boundary separating them, are determined during the solution (Zhang & Campbell 1992).

The laws governing the thermodynamic state of a moving granular material depend on the type of granular motion. For example, the granular temperature distribution

† Author to whom all correspondence should be addressed.

(T), is affected by different factors in shear-induced and vibrofluidized flows. In the former flows T is governed mainly by the kinetic energy exchange between the layers of granules moving with different average velocities. In the vibrofluidized motion the granular temperature is determined by the work performed on the granular system by the moving vessel.

In all granular flows both the thermodynamic state and the hydrodynamic properties are affected by the kinetic energy losses during particle collisions. This is the main factor distinguishing the behaviour of granular (non-conservative) systems from that of molecular (conservative) systems. In particular, no thermodynamic equilibrium may exist in granular systems, save in the trivial case of motionless particles (zero granular temperature). As such, the hydrodynamic collisional state is maintained by external agitations. The present series of studies is devoted to modelling the vibrofluidized motion of granular materials, where this agitation is effected by interactions between a vertically vibrating vessel and particles falling in a gravity field.

Collisional (vibrofluidized) granular motion is interesting from several practical points of view (Chlenov & Mikhailov 1972; Gutman 1968; Roberts 1984). First experimental studies demonstrated that the major part (if not all) of the layer moves as a single plastic block (Bachmann 1940; Kroll 1954; Gutman 1976). This phenomenon has formed the basis for a model which ignores relative particle motion (granular temperature) within this apparently solid block. This motion, however, is responsible for several important phenomena, including segregation of different particles (Ahmad & Smalley 1973) and circulative particle motion (Savage 1988).

Goldshtein *et al.* (1995*a*) showed that vibrofluidized granular systems are characterized by interacting transverse and compression–expansion waves, which propagate across the layers. These waves generate rapid collisional motion of granules which leads to their efficient mixing (Goldshtein *et al.* 1995*b*). The shock waves transform the bed into a gas-like state by supplying the energy of chaotic granular motion and creating collisional interactions. The expansion waves are responsible for conversion of chaotic granular kinetic motion into the translational (averaged) layer motion and the concomitant layer expansion. Therefore, investigation of these waves should be the basis of studies of vibrofluidization of granular layers.

Two methods are normally used for description of the collisional motion of granular materials, namely particle dynamic simulation (PDS) and continuum models. In PDS models trajectories of many particles are simultaneously calculated for specified interparticle interactions with subsequent averaging to obtain the effective macroscopic information of interest in each specific application. The continuum models are aimed at developing macroscopic (hydrodynamic) equations, governing corresponding effective properties of moving materials (e.g. granular pressure, temperature, density, etc.). This is done on the basis of the gas kinetic theory, modified to account for the kinetic energy dissipation during particle impacts. The continuum methods are physically illustrative, allowing application of the classical solution methods of mathematical physics and fluid mechanics. They can adequately reflect the complex microscopic information (about granular size, shape, mechanical properties, etc.) at the macroscale (hydrodynamic) level of description.

In recent years the vibrofluidization problem has been attacked using variants of the PDS models (Luding *et al.* 1994*a*; Luding, Herrmann & Blumen 1994*b*; Lan & Rosato 1995). In particular, with a one-dimensional vibrofluidization model Luding *et al.* (1994*a*) showed that the layer expansion is proportional to $(A\omega)^2/(1-e)$, where A and ω are the amplitude and the frequency of the vessel's vibrations and e is the granular restitution coefficient. This qualitatively confirms the result obtained in Part 2 of this

series (Goldshtein *et al.* 1995*a*) on the basis of a simple model of the wave propagation processes. Moreover, Lan & Rosato (1995) discovered periodic expansions and collapses of the bed occurring in phase with the vibrating vessel. This clearly may be attributed to the wave propagation, although this interpretation was not suggested by the authors.

Wave propagation phenomena may be observed only in granular systems containing sufficiently many particles. Simulation of such systems on computers is still a cumbersome and sometimes formidable task. The observation of waves in the above studies was precluded by the relatively small number of particles included in the system. Therefore, simulations of Lan & Rosato (1995) only confirmed the results of Bachmann (1940) and Clement & Rajchenbach (1991) about the possibility of vibrofluidizing no more than 5–6 particle monolayers. In addition, the spatial periodicity boundary conditions used by Lan & Rosato (1995) implied that an infinitely wide layer was treated. This precluded observation of the transverse gravitational waves experimentally found in Part 2.

The PDS methods are efficient provided that the number of particles and the collisional model adequately represent the system chosen for simulations. Verification of the PDS schemes may be done by comparing the numerical results with solutions of several simplified model problems, obtained by the continuum hydrodynamic equations. One such model problem is simple shear flow of a granular material in the absence of gravity and solid boundaries (Jenkins & Richman 1985, 1988; Lun & Savage 1987; Richman 1989; Lun 1991; Savage 1992; Lun & Bent 1994). Comparison of PDS solutions with the analytical results obtained for this flow for various collisional models enabled the understanding of the delicate energy balance within flowing granular materials.

So far no such solutions have been obtained for unsteady flows, in particular for the wavy motion of granular materials. This article and Goldshtein, Shapiro & Gutfinger (1996) (Part 3 of this series) are aimed at obtaining analytical solutions of such model problems. These solutions may be used to understand, rationalize and interpret experimental and computational results on vibrofluidized motion of vertical granular layers. Namely, in Part 3 we considered the compression of a cold granular gas by a moving solid piston. In this paper we treat the complementary problem of the expansion of an agitated granular gas into particle-free space.

Transformation of kinetic energy from the chaotic granular motion to directional motion (and vice versa) is the fundamental problem of wavy dynamics of granular materials. This problem has been studied in the classical gas dynamics theory (Courant & Friedrichs 1948). Such problems were neither treated nor even formulated for granular systems. The non-conservative nature of granular systems (kinetic energy dissipation) clearly exerts a strong influence on the kinetic energy transformation and dynamics of wave propagation. In particular, in Part 3 we have shown that only a finite part of a resting granular layer may be fluidized by a uniformly moving piston, no matter how large its velocity. This is in contrast with molecular gases where this part grows indefinitely with time. Similarly, the classical solution for expansion wave propagation in conservative systems cannot provide insight in the comparable physical processes occurring in the granular gas, even for an infinitesimally small energy dissipation rate.

Vibrofluidization is a process occurring in the gravity field, which acts to bring the layer down to meet the vessel. In Part 2 we investigated periodic vibrational regimes where the layer spends most of the time in free flight. Accordingly, this problem could be formulated and treated during one vibrational cycle between two subsequent

contacts with the bottom. After the contact a shock wave propagates upwards, which is followed by the layer detachment from the bottom of the vessel and its free flight motion, until it again meets the bottom. The expansion wave propagates downwards during the layer free flight, immediately after the shock wave reaches the uppermost part of the layer. This process may be described in the absence of gravity, which enables the physics of the kinetic energy conversion in the presence of energy dissipation to be elucidated. Investigation of these processes is necessary for describing the total kinetic energy balance, averaged over many vibrational cycles, and hence the whole vibrational state. The latter more general treatment should include the gravity force, which will be done in a subsequent study.

Shock and expansion wave propagation in molecular gases admits simple self-similar solutions (Courant & Friedrichs 1948). They serve as test problems for verification of more complicated analytical and numerical models (Moody 1990). The non-conservative nature of granular systems makes the problem of expansion wave propagation much more complicated than for molecular gases. From the mathematical point of view, dissipation of granular kinetic energy in flowing granular materials introduces a time scale which does not allow self-similar solutions to be obtained. In particular, a solution by series expansions in terms of a small parameter, characterizing weak energy dissipation, will not be uniformly valid for all times, and hence will be of limited use.

The paper is organized as follows. In §2 the equations and boundary conditions governing the problem of expansion wave propagation are formulated. In §3 several asymptotic solutions in the wave tail, wave head and intermediate regions are developed, respectively. Matching of all these solutions provides analytical expressions for the velocity, pressure and density within the whole wave region, which are uniformly valid for all times. In particular, in the limit of vanishing kinetic energy losses our solution reproduces the classical self-similar expansion wave solution (Courant & Friedrichs 1948). Section 4 is devoted to a discussion on several calculated parameters and a comparison with the approximate theory described in Part 2 of this series.

2. Problem formulation

2.1. *Euler's hydrodynamic equation*

Consider an ensemble of identical inelastic rough spherical granules of diameter σ, filling a semi-infinite spatial domain $x > 0$ separated from vacuum by a thin partition (see figure 1). The granules are assumed to be sufficiently heavy that the effect of the drag force (resulting from interactions with the surrounding granular gas) on their motion is negligible. At time $t = 0^+$ the partition is withdrawn and the gas expands into the vacuum along the x-axis (see figure 1).

We describe the expansion process in the Lagrangian coordinates in terms of the mass variable h, defined by

$$h = \int_{-\infty}^{x} \rho(\xi)\,\mathrm{d}\xi. \tag{1}$$

Neglecting gravitational force, as well as the gas thermal conductivity and viscosity, one can write the conservation equations for mass, momentum and energy in terms of h and the time variable t (Part 3):

$$\frac{\partial}{\partial t}\left(\frac{1}{\rho}\right) = \frac{\partial u}{\partial h}, \quad \frac{\partial u}{\partial t} + \frac{\partial P}{\partial h} = 0, \quad \frac{\partial}{\partial t}\left(\frac{E}{m}\right) + P\frac{\partial u}{\partial h} = I, \tag{2a–c}$$

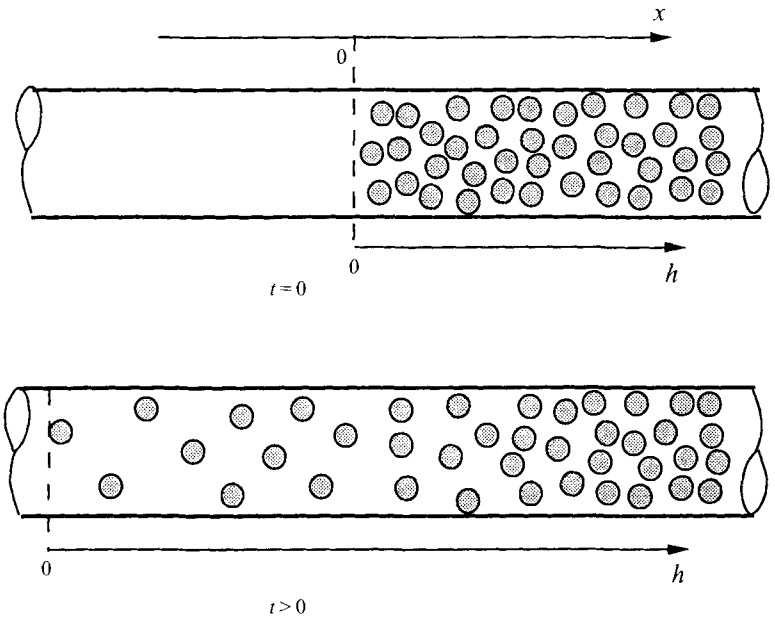

FIGURE 1. Schematic of the expansion wave propagation.

where $\rho = mn = \nu\rho_p$ is the bulk mass density, m and ρ_p are respectively the mass and mass density of individual particles, n is the particle number density, ν is the solid fraction (volume of solids per unit gas volume), u is the bulk velocity, E is the total energy of particle random motion, P is the hydrostatic granular pressure, and I is the volumetric sink term, accounting for losses of particle kinetic energy during collisions.

The above equations require constitutive relationships for the granular pressure and the sink term, relating them to other hydrodynamic quantities and mechanical properties of the colliding granules. Additionally, modelling of flows of rough particles requires knowledge of the energy partition between the translational and rotational modes.

In Part 1 of this series (Goldshtein & Shapiro 1995) constitutive relationships were found from the Chapman–Enskog solution of the Boltzmann equation, which was appropriately modified to include a fairly general particle collisional model. For dilute granular gases one can use this solution to express the gas hydrostatic pressure in the form

$$P = \tfrac{1}{2}nE\alpha_t. \tag{3}$$

The coefficient α_t depends on the particle restitution coefficient e and roughness β. For the particular cases of perfectly rough particles ($\beta = 1$) $\alpha_t = \frac{4}{3}$, and for absolutely smooth spheres ($\beta = -1$) $\alpha_t = \frac{2}{3}$ (see Appendix A of Part 3).

The sink term on the right-hand side of (2*c*) is given in Part 1, and for a dilute gas may be represented in the form

$$I = C_0\sigma^2 n\left(\frac{E}{m}\right)^{3/2} + \frac{\partial u}{\partial h}C_1 P, \tag{4}$$

where C_0, C_1 are functions of particle restitution coefficient e, and roughness, β (see (A 4)–(A 11) of Appendix A of Part 3).

2.2. *The speed of sound*

The speed of sound a, i.e. of propagation of infinitesimal disturbances through a dilute colliding granular gas, was calculated in Part 1 in the form

$$a^2 = \gamma \frac{P}{\rho}, \tag{5}$$

where

$$\gamma = 1 + \tfrac{1}{2}\alpha_t (1 - C_1). \tag{6}$$

It follows from (5) that for the evaluation of the speed of sound in a dilute granular gas one can use the standard expression for a polytropic gas with the adiabatic exponent γ given by (6). Values of α_t and C_1 appearing in (6) are defined by (A 1) and (A 5) of the Appendix of Part 3.

2.3. *Dimensionless problem formulation*

We now mark by a tilde the dimensional hydrodynamic properties. The corresponding non-marked letters denote dimensionless quantities defined using the initial density, $\tilde{\rho}_0$, granular pressure, $\tilde{P}_0$, kinetic energy $\tilde{E}_0$, and the associated speed of sound, $\tilde{a}_0$, as the reference values, i.e.

$$\rho = \tilde{\rho}/\tilde{\rho}_0, \quad P = \tilde{P}/\tilde{P}_0, \quad u = \tilde{u}/\tilde{a}_0, \quad h = \tilde{h}\sigma^2/m, \quad t = \tilde{t}\sigma^2\tilde{\rho}_0\tilde{a}_0/m. \tag{7a–e}$$

Using (5) for the speed of sound, the equation of state (3) and (4), (7a–e), one can rewrite the hydrodynamic equations (2a–c) in the dimensionless forms:

$$\frac{\partial}{\partial t}\left(\frac{1}{\rho}\right) = \frac{\partial u}{\partial h}, \quad \frac{\partial u}{\partial t} + \frac{1}{\gamma}\frac{\partial P}{\partial h} = 0, \quad \rho\frac{\partial P}{\partial t} - \gamma P\frac{\partial \rho}{\partial t} = -2\delta(\rho P)^{3/2}, \tag{8a–c}$$

where

$$\delta = -\tfrac{1}{2}C_0(2/\gamma\alpha_t)^{1/2} \tag{8d}$$

is the parameter characterizing kinetic energy losses.

Continuous (i.e. without discontinuities of hydrodynamic properties) flows of molecular gases are usually described in the isentropic approximation. Moreover, for such flows the energy balance equation may be integrated to express the gas pressure in terms of the density (Courant & Friedrichs 1948).

The entropy function may also be introduced for granular gases. However, owing to kinetic energy losses neither this quantity nor the energy of random granular motion are conserved. This precludes closed-form integration of the energy balance equation for granular gases. Nevertheless, we will utilize several integral forms of the energy equation which will prove helpful in the subsequent analyses. It may be shown that the expression

$$P(t, h) = \rho^{\gamma}(t, h)/S^2(t, h, \rho), \tag{9}$$

where

$$S(t, h, \rho) = C_s(h) + \delta \int_0^t \rho^{(\gamma+1)/2}(\eta, h)\, \mathrm{d}\eta, \tag{10}$$

obeys (8c). Expressions (9) and (10) are generalizations of the entropy conservation integrals for the case of inelastically colliding particles. It is clear that in the special case of conservative gases (i.e. $\delta = 0$) the function $C_s(h)$ characterizes the initial entropy distribution in the system. These equations are further used in §3.3.

Boundary conditions for (8) are formulated from the following considerations. Owing to the instantaneous pressure drop at $t = h = 0$ a rarefaction wave propagates

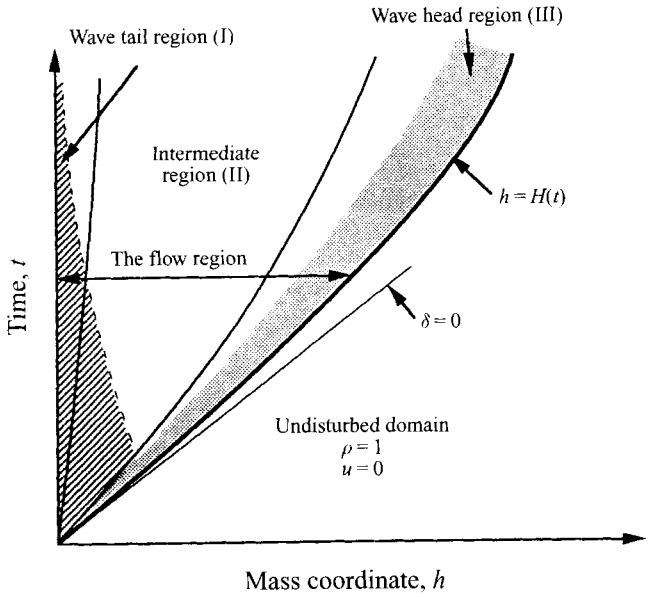

FIGURE 2. Domains of the various solutions developed for the expansion wave problem.

from the boundary into the granular gas. Those particles which the front has reached are disturbed from their initial state of hydrodynamic (but not thermodynamic) rest. The wave front travels with the speed of sound a in the undisturbed domain. Owing to granular energy dissipation only the density and (zero) bulk velocity within the undisturbed domain will be conserved, while the granular pressure, kinetic energy and speed of sound will diminish. In these conditions system (8) yields the following solution:

$$\rho = 1, \quad P = (1+\delta t)^{-2}, \quad u = 0, \quad a = (1+\delta t)^{-1}. \tag{11a–d}$$

It follows from (11d) that the trajectory of the rarefaction wave front is

$$H(t) = \int_0^t a(\tau)\,\mathrm{d}\tau = \frac{\ln(1+\delta t)}{\delta}. \tag{12}$$

The granular flow resulting from the expansion of a granular gas into vacuum is, thus, contained within the region $0 < h < H(t)$ (see figure 2). Since this region is adjacent to the undisturbed domain, the solution at the wave head $h = H(t)$ should obey conditions (11a–d). On the other hand, at the wave tail, $h = 0$, the pressure is $P = 0$.

3. Solution

3.1. *General*

We solve equations (8a–c) by employing a perturbation method (Van Dyke 1968), considering three separate asymptotic solutions: (I) Wave tail expansion (see §3.2), (II) intermediate expansion far from the boundaries (§3.3) and (III) wave head expansion (§3.4) (see figure 2). In §3.5 these separate solutions will be combined into a single matched composite solution.

3.2. *Wave tail asymptotic solution*

In the absence of granular energy dissipation (conservative gasses, $\delta = 0$), problem (8*a–c*) has the following self-similar solution (Courant & Friedrichs 1948):

$$\rho_c = \zeta^{2/(\gamma+1)}, \quad P_c = \rho_c^{\gamma}, \quad u_c = -U_{esc}(1-\zeta^{(\gamma-1)/(\gamma+1)}), \quad \zeta = \frac{h}{t}, \tag{13a–d}$$

where

$$U_{esc}(\gamma) = \frac{2}{\gamma-1} \tag{13e}$$

is the dimensionless velocity of a gas escaping into vacuum. One can expect that in the close vicinity of the wave tail ($h \ll 1$), where pressure P and density ρ are small, the effect of the sink term appearing on the right-hand side of the energy conservation equation (8*c*) is negligible and the expansion of the granular gas differs slightly from that of the conservative gases described by (13*a–d*). Bearing in mind the above reasoning, we seek a small-coordinate ($h \ll 1$) expansion in the form

$$\rho_T = \rho_T^{(0)} + \rho_T^{(1)} + \ldots, \quad u_T = u_T^{(0)} + u_T^{(1)} + \ldots, \quad P_T = P_T^{(0)} + P_T^{(1)} + \ldots, \tag{14a–c}$$

where

$$\rho_T^{(0)}/\rho_T^{(1)} \ll 1, \quad u_T^{(0)}/u_T^{(1)} \ll 1, \quad P_T^{(0)}/P_T^{(1)} \ll 1, \ldots. \tag{15a–c}$$

A more accurate estimation of the validity range of expansions (14), where (15*a–c*) hold, is given below.

Substituting (14*a–c*) into 8(*a–c*) and using (15) one finds that (8*a*, *b*) for the leading terms are unchanged and identical to those of the conservative gas, whereas (8*c*) adopts the form

$$\rho_T^{(0)} \frac{\partial P_T^{(0)}}{\partial t} - \gamma P_T^{(0)} \frac{\partial \rho_T^{(0)}}{\partial t} = -2\delta(\rho_T^{(0)} P_T^{(0)})^{3/2}.$$

Analysis of this equation shows that for $h \ll 1$ (at the wave tail) $\rho_T^{(0)} \ll 1$, $P_T^{(0)} \ll 1$. Therefore its right-hand side is much smaller than the left-hand side and may be neglected. We thus obtained that the leading-order terms in (14*a–c*) satisfy the equations for the conservative gas (albeit with $\gamma = \gamma(e, \beta)$). Consequently

$$\rho_T^{(0)} = \rho_c, \quad u_T^{(0)} = u_c, \quad P_T^{(0)} = P_c, \tag{16a–c}$$

where ρ_c, u_c, P_c are given by the (13*a–c*). U_{esc}, given by (13*e*), is the escape velocity of the granular gas, where the influence of the granular collisional properties is embodied within the specific heat ratio $\gamma = \gamma(e, \beta)$. Physically this coincidence is explained by noting that at the initial moment the outermost granules (wave tail) instantaneously escape into vacuum without kinetic energy losses.

Substituting (13*a–c*)–(16*a–c*) into (8*a–c*) and using the standard perturbation technique (Van Dyke 1968), one obtains after some algebraic manipulations the first-order correction of the wave tail asymptotic solution in the form

$$\rho_T^{(1)} = h\zeta^{2/(\gamma+1)}(A_\rho + B_\rho \ln t), \quad u_T^{(1)} = h\zeta^{(\gamma-1)/(\gamma+1)}(A_u + B_u \ln t), \tag{17a, b}$$

$$P_T^{(1)} = h\zeta^{2\gamma/(\gamma+1)}(A_p + B_p \ln t), \tag{17c}$$

where

$$A_p = \gamma A_\rho, \quad B_p = \gamma B_\rho - 2\delta, \tag{18a, b}$$

$$A_u = -\frac{1}{\gamma}A_\rho - \frac{\gamma+1}{2\gamma}B_\rho, \quad Bu = -\frac{1}{\gamma}A_\rho, \tag{18c, d}$$

$$A_\rho = \frac{(\gamma+1)(3-\gamma)}{6\gamma^2+4\gamma-2}B_\rho, \quad B_\rho = \frac{(6\gamma+2)\,\delta}{3\gamma^2+2\gamma-1}. \tag{18e, f}$$

It follows from (17*a–c*), (18*a–f*), (13*a–c*) and (16*a–c*) that straightforward coordinate expansions (14*a–c*) satisfy conditions (15*a–c*) for $h \ll 1$. Moreover, since all coefficients in (18) are proportional to δ, conditions (15*a–c*), require that $h\delta \ln t \ll 1$. Therefore, the domain in which the solution (17) is valid diminishes with time. Convergence of the series (14*a–c*) is discussed in the following section.

3.3. *Intermediate asymptotic solution*

Here we construct an approximation of the wave solution valid for large times. Consider an arbitrary material point within the disturbed range. Under the action of the gas pressure gradient, directed from the head to the tail of the expansion wave, the particles will accelerate and the energy of their random motion will transform into the energy of their average motion. Solution (13*a–d*) predicts that the hydrodynamic velocity of the conservative gas approaches its large-time limit. This is the speed of escape $U_{esc}(\gamma)$ which is independent of the coordinate h. On the other hand, within the granular gas, dissipation of the granular kinetic energy obviously leads to a non-uniform large-time finite particle velocity $U^{\infty}(h;\delta)$, that is

$$\lim_{t\to\infty} u(t,h;\delta) = U^{\infty}(h;\delta). \tag{19a}$$

However, as the parameter δ, which characterizes the intensity of the dissipation process, vanishes, the above limiting value reduces to U_{esc}, i.e.

$$U^{\infty}(h;\delta)|_{\delta=0} = U_{esc}(\gamma).$$

On the other hand, for any δ, the uppermost particles will have the same velocity as the conservative gas (with the same γ), that is

$$U^{\infty}(h;\delta)|_{h=0} = U_{esc}(\gamma).$$

Subject to *a posteriori* verification, we assume that U^{∞} depends upon the single variable $h\delta$, i.e.

$$U^{\infty}(h;\delta) = U^{\infty}(h\delta). \tag{19b}$$

This assumption will be justified in §3.5 by matching of the solutions obtained in domains I, II and III.

It is now convenient to introduce new variables:

$$x = h\delta, \quad \tau = 1 + t\delta, \tag{20a, b}$$

in terms of which (8*a–c*) may be rewritten in the form

$$\frac{\partial}{\partial\tau}\left(\frac{1}{\rho}\right) = \frac{\partial u}{\partial x}, \quad \frac{\partial u}{\partial\tau} + \frac{1}{\gamma}\frac{\partial P}{\partial x} = 0, \quad \rho\frac{\partial P}{\partial\tau} - \gamma P\frac{\partial P}{\partial\tau} = -2(\rho P)^{3/2}. \tag{21a–c}$$

This system is to be solved for $x \geqslant 0$ and $\tau \geqslant 1$, subject to the boundary conditions

$$\rho = 1, \quad u = 0, \quad P = \tau^{-2} \quad \text{for} \quad x = \ln\tau, \tag{22a–c}$$

obtainable from (11*a–c*) combined with (12), (20*a*, *b*).

Substituting the asymptotic spatial function $U^{\infty}(x)$, given by (19*b*) into (21*a*) and integrating the resulting equation, one obtains the following large-time relationship for $\rho_M^{-1}(x)$:

$$\rho_M^{-1}(x) = \tau\frac{\mathrm{d}}{\mathrm{d}x}U^{\infty}(x) + o(\tau), \quad \tau\to\infty.$$

Substitution of this expression into (21*c*) results in

$$P_M(\tau, x) = \tau^{-\gamma} \Pi_M^{(0)}(x) + o(\tau^{-\gamma}), \quad \tau \to \infty.$$

Continuing the above procedure one can arrive at the following large-time ($\tau \gg 1$) asymptotic expansions:

$$u_M(\tau, x) = U_M^{(0)}(x) + U_M^{(1)}(x)\tau^{1-\gamma} + \ldots, \tag{23a}$$

$$\rho_M^{-1}(\tau, x) = R_M^{(0)}(x)\tau + R_M^{(1)}(x)\tau^{2-\gamma} + \ldots, \tag{23b}$$

$$P_M(\tau, x) = \Pi_M^{(0)}(x)\tau^{-\gamma} + \Pi_M^{(1)}(x)\tau^{(1-3\gamma)/2} + \ldots, \tag{23c}$$

where the zero-order term $U_M^{(0)}(x)$ in the expansion (23*a*) represents the large-time, ultimate, hydrodynamic velocity $U^{\infty}(x)$ (appearing in (19*b*)) to be determined in the course of the solution. Upon substitution of (23*a–c*) into (21*a–c*), one obtains the following relations:

$$R_M^{(0)}(x) = \frac{\mathrm{d}}{\mathrm{d}x} U_M^{(0)}(x), \quad \Pi_M^{(1)}(x) = \frac{4}{\gamma - 1} [R_M^{(0)}(x)]^{-1/2} [\Pi_M^{(0)}(x)]^{3/2}, \tag{24a, b}$$

$$U_M^{(1)}(x) = \frac{1}{(\gamma - 1)\gamma} \frac{\mathrm{d}}{\mathrm{d}x} \Pi_M^{(0)}(x), \quad R_M^{(1)}(x) = \frac{1}{2 - \gamma} \frac{\mathrm{d}}{\mathrm{d}x} U_M^{(1)}(x), \tag{24c, d}$$

imposed on the unknown coefficient functions in expansions (23).

The above relations are insufficient for the determination of the six functions appearing in (23*a–c*). Formally one can express any four functions in (23) in terms of the other two remaining functions; for example, one can express $U_M^{(1)}(x), R_M^{(1)}(x), \Pi_M^{(1)}(x), R_M^{(0)}(x)$ via $\Pi_M^{(0)}(x), U_M^{(0)}(x)$. However, any attempt to determine the latter two functions directly from the boundary conditions at the wave tail and head involves the following difficulties. Expansions (23 *b*, *c*) predict that the particle density and pressure decrease as τ^{-1} and $\tau^{-\gamma}$, respectively. These solutions cannot be matched with (13*a–d*) which are the leading solutions of the wave tail expansion (14*a–c*). Moreover, one can see that the leading term of expansion (23*c*) cannot satisfy boundary condition (22*c*). Indeed an attempt to satisfy this condition yields $\Pi_M^{(0)}(x) \sim e^{(\gamma-2)x}$, which is physically non-plausible since $\gamma - 2 < 0$ and, hence, the above result predicts a monotonic pressure decrease with increasing h.

Summarizing the above, one can state that the system (24*a–d*) cannot be mathematically closed by matching solutions (23*a–c*) with the wave tail and the wave head boundary conditions. In order to overcome this difficulty, in §3.4 we construct a matched composite solution. This solution will be *inter alia* matched with leading terms of (23*a–c*). The validity range of this matched composite solution will be shown to be wide enough to allow determination of the function $U_M^{(0)}$ by a matching procedure. Then the leading terms in the density and pressure expansions will be respectively obtained from (24*a*) and the integral form of the energy balance equation (see §§3.1, 3.4).

The leading term of the intermediate asymptotic solution (23*a–c*) describes the final stage of evolution of the expansion wave, when almost all the energy of the chaotic granular motion is transformed into the energy of the average granular motion and is partly dissipated due to the non-conservative nature of particle collisions. At this stage of evolution each particle moves with a time-independent (albeit x-dependent) speed $U^{\infty}(x)$. Hence, (23*a–c*) is not valid in the wave head domain, where particles accelerate towards U^{∞}. This genesis of the hydrodynamic motion, which for each particle begins after the rarefaction wave front reaches it, is treated in the following section.

3.4. *Head wave asymptotic solution*

We now rewrite (9) and (10) in terms of the variables τ, x, given by (20 *a*, *b*):

$$P(\tau, x) = \rho^{\gamma}(\tau, x)/S^2(\tau, x, \rho), \tag{25a}$$

$$S(\tau, x, \rho) = C_s(x) + \int_1^{\tau} \rho^{(\gamma+1)/2}(\eta, x)\,\mathrm{d}\eta. \tag{25b}$$

These equations in combination with conditions (22*a–c*) imply that

$$C_s(x) = 1. \tag{26}$$

Indeed, to demonstrate the above we rewrite (25*a*) in the following form:

$$S(\tau, x, \rho) = C_s(x) + \int_1^{e^x} \rho^{(\gamma+1)/2}(\eta, x)\,\mathrm{d}\eta + \int_{e^x}^{\tau} \rho^{(\gamma+1)/2}(\eta, x)\,\mathrm{d}\eta. \tag{27a}$$

Since in the undisturbed domain $x > \ln\tau$, the particle density $\rho = 1$ (see (22*a*)) (27*a*) becomes

$$S(\tau, x, \rho) = C_s(x) + e^x - 1 + \int_{e^x}^{\tau} \rho^{(\gamma+1)/2}(\eta, x)\,\mathrm{d}\eta. \tag{27b}$$

Substituting S from (27*b*) into (25*a*), using boundary conditions (22*a*, *c*) and observing that the second integral on the right-hand side of (27*b*) vanishes at the wave head $\tau = e^x$, one obtains the required equation (26).

Equations (26) and (27*b*) yield

$$S(\tau, x, \rho) = e^x + \int_{e^x}^{\tau} \rho^{(\gamma+1)/2}(\eta, x)\,\mathrm{d}\eta. \tag{28}$$

The integral form of the energy equation represented by (25*a*), (28) is valid within the whole disturbed domain, namely for $\tau > e^x$ (see figure 2). In the immediate vicinity of the wave head, i.e. where

$$\epsilon(\tau, x) \equiv 1 - e^x/\tau \ll 1, \tag{29}$$

(28) may be simplified. Using the fact that ρ is close to unity when $\epsilon \ll 1$, one can rewrite (28) in the following form:

$$S(\tau, x) = \tau\{1 + \tfrac{1}{2}\epsilon(\tau, x)[\rho^{(\gamma+1)/2}(\tau, x) - 1]\}. \tag{30}$$

This equation together with (25*a*) is used below in the derivation of the wave head approximation.

Consider the wave head domain defined by inequality (29). In this region we seek a solution of the problem (21)–(22) in the form of the following Taylor expansions:

$$\rho(\tau, x) = 1 + \rho_H^{(1)}(\tau)\epsilon + \rho_H^{(2)}(\tau)\epsilon^2 + O(\epsilon^3), \tag{31a}$$

$$u(\tau, x) = u_H^{(1)}(\tau)\epsilon + u_H^{(2)}(\tau)\epsilon^2 + O(\epsilon^3), \tag{31b}$$

with the pressure $P(\tau, x)$ expressed via the functions $\epsilon(\tau, x), \rho(\tau, x)$ by (25*a*) and (30). It is obvious that the above solution forms satisfy conditions (22*a–c*) imposed at the wave head.

For the evaluation of the unknown functions $\rho_H^{(i)}(\tau), u_H^{(i)}(\tau)$ $(i = 1, 2, \ldots)$ substitute expansions (31*a*, *b*) into (21*a*, *b*), (25*a*), (30) to obtain:

first-order approximation

$$u_H^{(1)}(\tau) = \rho_H^{(1)}(\tau)/\tau; \tag{32}$$

second-order approximation

$$\frac{\mathrm{d}}{\mathrm{d}\tau}\rho_H^{(1)}(\tau) = \frac{2}{\tau}[(\rho_H^{(1)}(\tau))^2 - \rho_H^{(2)}(\tau)] + 2u_H^{(2)}(\tau), \tag{33a}$$

$$\frac{\mathrm{d}}{\mathrm{d}\tau}u_H^{(1)}(\tau) = \frac{1}{\tau}\left[\left(\frac{\gamma-1}{\tau}\right)(\rho_H^{(1)}(\tau))^2 - \left(\frac{\gamma+1}{\gamma\tau}\right)\rho_H^{(1)}(\tau) + \left(\frac{2}{\tau}\right)\rho_H^{(2)}(\tau) - 2u_H^{(2)}(\tau)\right]. \tag{33b}$$

Functions $u_H^{(2)}, \rho_H^{(2)}$ may be simultaneously excluded by adding (33*a*, *b*). The resulting equation combined with (32) yields the following ordinary differential equation for $\rho_H^{(1)}$:

$$\frac{\mathrm{d}}{\mathrm{d}\tau}\rho_H^{(1)}(\tau) = \frac{1}{\tau}\left[\left(\frac{\gamma+1}{2}\right)\left(\rho_H^{(1)}(\tau)\right)^2 - \left(\frac{1}{2\gamma}\right)\rho_H^{(1)}(\tau)\right], \tag{34}$$

the solution of which is

$$\rho_H^{(1)}(\tau) = [\gamma(\gamma+1)(1-c\tau^{1/2\gamma})]^{-1}, \tag{35}$$

where c is an arbitrary constant.

With $\rho_H^{(1)}$ given above, one can rewrite the asymptotic solution for the wave head given by (31*a*, *b*), (25), (30) up to the terms of $O(\epsilon)$:

$$\rho(\tau, x) = 1 + \rho_H^{(1)}(\tau)\,\epsilon + O(\epsilon^2), \tag{36a}$$

$$u(\tau, x) = \rho_H^{(1)}(\tau)\,\epsilon/\tau + O(\epsilon^2), \tag{36b}$$

$$P(\tau, x) = [1 + \rho_H^{(1)}(\tau)\,\epsilon/\tau]^{\gamma}\tau^{-2} + O(\epsilon^2). \tag{36c}$$

The above scheme can be employed to obtain higher-order terms in expansions (31). However, solution (36*a–c*) will prove sufficient for constructing the general matched composite solution of the problem, which will be done in §3.5.

3.5. *Matched composite solution*

Each of the separate asymptotic solutions (14), (23), (36), respectively obtained in §§3.1, 3.2, 3.3, gives only a partical description of the hydrodynamic properties in the disturbed region. The goal of the following treatment is to describe variations of these quantities throughout the whole disturbed region by combining the above separate expansions into a single matched composite solution u_s, ρ_s and P_s. The solution for the velocity u_s is constructed in the following self-similar form (cf. (13*c*)):

$$u_s(\tau, x) = U(x)(1 - \eta^{(\gamma-1)/(\gamma+1)}), \tag{37}$$

where η is a self-similar variable

$$\eta = \frac{e^x - 1}{\tau - 1}. \tag{38}$$

The functional form of (37) and (38) can be substantiated by the following observations. First, one can use definitions (20*a*, *b*) to verify that (37), (38) satisfies boundary condition (22*b*) at the wave head. Secondly, in the limit of the conservative gas (i.e. $\delta \to 0$) η approaches the self-similar variable ζ, given by (13*d*), which appears in the corresponding solution (13*a–c*). By virtue of (19*b*) and (20*a*), in the limit $\delta \to 0$ x vanishes together with δ, and the following condition should, thus, be imposed:

$$U(x) \to -U_{esc}(\gamma) \quad \text{for} \quad x \to 0. \tag{39}$$

In the limit $\delta \to 0$ this condition provides a smooth transition between the matched composite solution (37), (38) for the dissipative granular gas and the wave tail solution

(16*b*). Thirdly, the same transition may be also seen to exist for $x \to 0$ by virtue of the choice of the self-similar variable η. Indeed, it follows from (20*a*, *b*) and (38) that $\eta \approx \zeta$ for small x. Consequently, (37), (38) together with condition (39) yield the zero-order term (16*b*), (13*c*) of the wave tail asymptotic expansion (14*b*).

In the limit $\tau \to \infty$ (x-fixed) the matched composite solution (37), (38) reduces to the function $U(x)$, which, according to the intermediate expansion (23*a*), is the terminal hydrodynamic particle velocity $U^{\infty}(x)$.

Now we match the solution (37) with the wave head expansion (36*b*) at $\epsilon \to 0$. Using the matched asymptotic expansions scheme (Van Dyke 1968) we determine $U(x)$ by imposing the following matching condition:

$$u_s(\tau, x) \to \epsilon \rho_H^{(1)}(\tau)/\tau \quad \text{for} \quad \epsilon \to 0, \tag{40}$$

where $\rho_H^{(1)}(\tau)$ and ϵ are defined by (35) and (29), respectively. After some algebraic manipulations (29), (35), (37) and (38) combined with condition (40) yield

$$U(x) = \frac{e^x - 1}{\gamma(\gamma-1)e^{2x}(1 - ce^{x/2\gamma})}. \tag{41a}$$

The constant c appearing above, which determines also the wave head solution (35) and (36) is determined from the wave tail matching condition (39), which gives

$$c = 1. \tag{41b}$$

The above value of c together with (37), (38) and (41), completely determine the matched composite solution for the hydrodynamic velocity u_s:

$$u_s(\tau, x) = \frac{e^x - 1}{\gamma(\gamma-1)e^{2x}(1 - e^{x/2\gamma})}\left[1 - \left(\frac{e^x - 1}{\tau - 1}\right)^{(\gamma-1)/(\gamma+1)}\right]. \tag{42}$$

This expression constitutes the principal result of our analysis. The corresponding matched composite solution for mass particle density ρ_s, may be derived from the above solution for u_s, mass conservation equation (21*a*) and condition (22*a*) for density ρ at the wave head:

$$\frac{1}{\rho_s(\tau, x)} = 1 + U'(x)(1-\eta)(\tau - 1) - (\eta^{-2/(\gamma+1)} - 1)[\tfrac{1}{2}(\gamma-1)\,U(x)e^x + \tfrac{1}{2}(\gamma+1)(e^x - 1)\,U'(x)], \tag{43}$$

where

$$U'(x) \equiv \frac{\mathrm{d}}{\mathrm{d}x}U(x). \tag{44}$$

The matched composite solution for ρ_s consists of three additive terms, appearing on the right-hand side of (43). It may be shown that the first of them represents the wave head asymptotic solution (36*a*), the second the intermediate solution (23*b*), and the third the wave tail solution (14*a*). The sum of the second and third terms provides the first-order contribution with respect to the small parameter ϵ in the asymptotic expansion given by (35) and (36*a*).

The last step in the derivation of the matched composite solution is calculation of the granular pressure P_s. This may be performed after substitution of (43) into relations (25*a*), (28). However, the final expression for P_s obtained in such a way is complicated. Instead, we perform these calculations using a less accurate but simpler and more convenient expression for the density ρ_s. Towards this goal we discard the last term in (43), thereby obtaining

$$\rho_s(\tau, x) = [1 + U'(x)(\tau - e^x)]^{-1}. \tag{45}$$

This expression upon substitution into (28) for $S(\tau, x, \rho)$ and integration yields

$$S(\tau, x, \rho_s) = e^x + \frac{2}{\gamma - 1}[U'(x)]^{-1}[1 - \rho_s^{(\gamma-1)/2}(\tau, x)]. \tag{46}$$

The above expression together with relation (25*a*) yield the following approximation for the pressure P_s:

$$P_s(\tau, x) = \rho_s^{\gamma}(\tau, x)/S^2(\tau, x, \rho_s), \tag{47}$$

where $\rho_s(\tau, x)$ given by (45).

The approximate solutions for the density and pressure given by (45)–(47) satisfy the boundary conditions at the head wave and give the leading terms of the intermediate asymptotic solution (23*b*, *c*). However, they do not accurately reproduce the leading term (13*a*, *b*) of the wave tail asymptotic solution (14*a*, *b*), since the term responsible for the latter solution was neglected in (43). The region in which the wave tail asymptotic solution is valid diminishes with time (see the restrictions imposed on this solution at the end of §3.1), while the range of applicability of the approximation (45) for density ρ_s and, consequently, approximation (46), (47) for pressure P_s grows with time (see figure 2).

4. Results

Analysis of solution (42) and (43) shows that it satisfies the governing equations (8) both for small and large times, as well as the boundary condition imposed on the hydrodynamic properties for all times. In that sense one can consider this solution to be uniformly valid for all times. In particular, the intermediate domain, the solution for which was developed in §3.3 for apparently long times, in fact does not exist for small times. Indeed one can see that at the limit of $t \ll 1$, and hence $x \ll 1$, (42) simultaneously reproduces both the wave tail and the wave head solutions. This is also shown in figure 2, where the wave head and the wave tail domains are shown to overlap. Physically this overlap is explained by the observation that for any given $0 < e < 1$ and $|\beta| < 1$, there exists a short time period where the kinetic losses do not exert any significant influence on the flow regime.

Solutions (42) and (43) may be used to calculate the curves $\phi_\rho(\tau, x) = C_\rho = \text{const}$, $\phi_u(\tau, x) = C_u = \text{const}$, on which the velocity and density are conserved. These curves for smooth particles in the (x, τ) plane are plotted in figure 3(*a*, *b*). One can see that for small τ these curves coincide with the dashed straight lines of the classical solution (13*a*–*d*). These curves are plotted here in x, t coordinates using the expressions

$$C_\rho = \text{const} = \left(\frac{h}{t}\right)^{2/(\gamma+1)} = \left(\frac{x}{\tau - 1}\right)^{2/(\gamma+1)}, \tag{48}$$

$$C_u = U_{esc}[1 - C_\rho^{(\gamma-1)/2}]. \tag{49}$$

The solid lines in figure 3(*a*, *b*) exhibit the effect of inelastic particle collisions, which is embodied in the appropriately deformed dimensionless time and mass coordinates x and τ via parameter δ. Note that for smooth particles the adiabatic exponent γ is independent of restitution coefficient and equals $\frac{5}{3}$.

During a relatively short initial period the characteristic lines for non-conservative granular gases coincide with those for molecular gases. This time period is inversely proportional to δ; in particular, for almost conservative granules this period is long, i.e. of order $\delta^{-1} = (1 - e)^{-1}$. Therefore, for any particle restitution coefficient there exists an

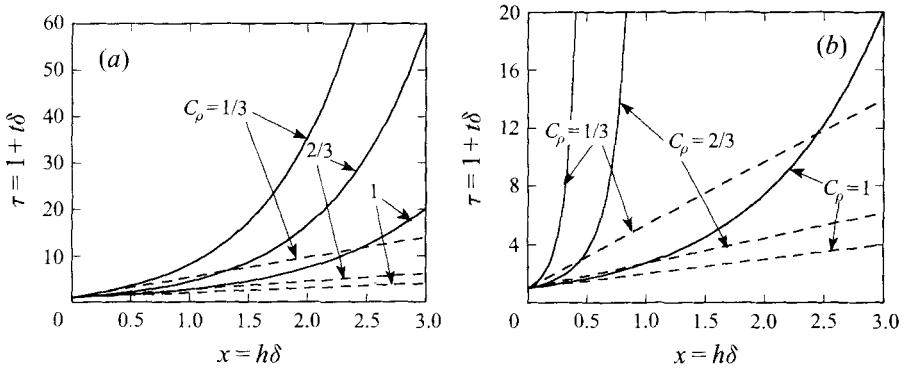

FIGURE 3. (*a*) Curves of constant density ($\phi_\rho = C_\rho = \text{const}$) for granular gas of smooth spheres ($\beta = -1$), drawn in the dimensionless time–mass coordinates. Dashed straight lines: classical solution (13*a*), $e = 1$. Curved lines: solution (43) $0 < e < 1$. (*b*) As (*a*) but for constant velocity ($\phi_u = C_u = \text{const}$). Dashed straight lines: classical solution (13*c*), $e = 1$. Curved lines: solution (42) $0 < e < 1$ plotted for $C_u = 2[1 - C_\rho^{(\gamma-1)/2}]/(\gamma - 1)$, for $C_\rho = 1, \frac{2}{3}$ and $\frac{1}{3}$.

initial (physical) time period during which the curves $\rho = \text{const}$ are straight lines. In the course of time these curves progressively deviate towards larger times. For large times τ (and x) these curves behave like exponents (see (50) below). This deviation is explained by the dissipation of the granular kinetic energy with the concomitant diminution of the speed of sound.

For molecular gases the characteristics serve as curves on which both density and velocity are conserved. In contrast, the curves ϕ_ρ, ϕ_u for the granular gases are different. Figure 3(*b*) shows the curves ϕ_u, plotted for constant values of $u = C_u$, corresponding to the values of C_ρ shown in figure 3(*a*). These curves differ markedly from the lines $\phi_\rho = \text{const}$ shown in figure 3(*a*). In particular, for long times ϕ_u have asymptotes $x = x_{max}$. The value of x_{max} decreases with increasing C_u. That is, all particles with mass coordinates $x > x_{max}$ cannot reach velocities larger than the corresponding $C_u = U(x_{max})$, where U is given by (41*a*, *b*). It also follows from the above formulae that $x_{max} \to \infty$ as $C_u \to 0$. Therefore, the limiting curve $C_u = 0$ corresponding to the wave head is the only one that has no asymptote.

The data shown in figure 3(*a*, *b*) are valid for smooth particles, in which case the result may be represented in a universal form, i.e. by the same curves for all values of e. In a more general situation, i.e. where $|\beta| < 1$, the specific heat ratio $\gamma = \gamma(e, \beta)$ and, hence, each set of particle collisional properties, requires a separate plot. Nevertheless, for large times one can use the approximate form (45) of the solution for ρ_s to calculate ϕ_ρ in the form

$$\tau = \left(\frac{1}{C_\rho} - 1\right)[U'(x)]^{-1} + e^x, \tag{50}$$

with $C_\rho \in (0, 1)$, on which the density ρ_s of the granular gas is conserved. In contrast, no curves exist on which the granular pressure is conserved. In particular, in (49) P_s decreases with x as (see (45–47)):

$$P_s(\tau, x) = C_\rho^\gamma \left[e^x + \left(\frac{2}{\gamma - 1}\right)(1 - C_\rho)/U'(x)\right]^{-2}, \tag{51}$$

where $U'(x)$ is given by (41*a*, *b*) and (44).

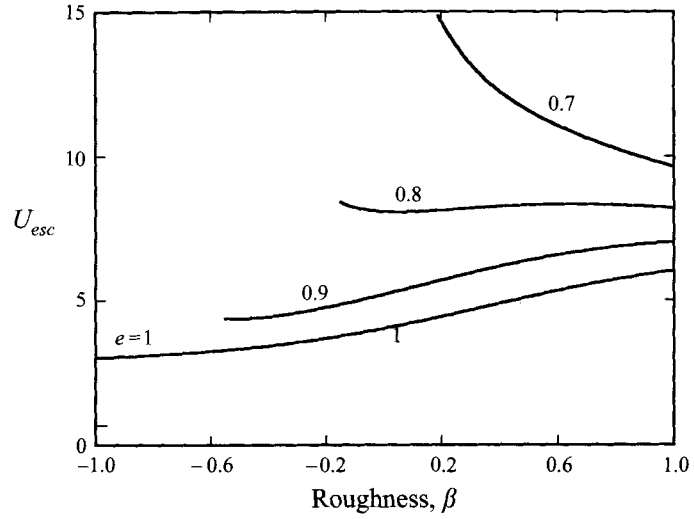

FIGURE 4. Dependence of the escape velocity U_{esc} on particle collisional properties.

Figure 4 shows the dimensionless escape velocity $U_{esc} = 2/(\gamma - 1)$ of a granular gas into vacuum *vs.* particle roughness for several values of the restitution coefficient e. The curve for $e = 1$ describes monotonic change of U_{esc} from $U_{esc} = 3$ for smooth to $U_{esc} = 6$ for rough particles. The effect of particle kinetic energy losses is still implicitly embodied within the adiabatic exponent γ, which is present both in the right-hand side of the expression for U_{esc} and in the speed of sound (5) and (6) normalizing it (see (7*c*)). This speed of sound decreases with decreasing e (Part 1). In addition, with decreasing e (increasing restitution coefficient) the granular random kinetic energy is redistributed in favour of the rotational degrees of freedom, which leads to a decrease of the adiabatic exponent γ and the concomitant increase of U_{esc} (see the curves for $e = 0.7$–0.9). Thermodynamically, this redistribution is equivalent to an increase of the gas specific heat and, hence, internal energy, which is retrieved as the kinetic energy of the escaping (freely flowing) gas.

The effect of kinetic energy losses on U_{esc} is manifested in a two-fold manner: by means of redistribution of the granular temperature between the rotational and translational degrees of freedom (via α_t in (6)) and by direct losses, associated with the work of the pressure forces, via C_1 in (6) (see Part 1). These losses are relatively low for $e \sim 1$. In these cases U_{esc} decreases monotonically, mainly due to α_t increasing with β where β decreases from 1 (see figure 1 of Part 1). One should also note that for lower e, α_t depends weakly on β. In this case γ is affected mainly by C_1, the effect of which is to increase γ with increasing frictional losses (β decreasing from 1). This is shown in figure 4 (see curve for $e = 0.7$).

We next calculate the ultimate escape kinetic energy and momentum of the expanding layer, i.e. the kinetic energy and momentum of the hydrodynamic motion, gained by the accelerating particles

$$E^{\infty} = \frac{1}{2}\int_0^{\infty} u^2(t,h)|_{t\to\infty}\,\mathrm{d}h, \quad M^{\infty} = \int_0^{\infty} |u(t,h)|_{t\to\infty}\,\mathrm{d}h, \tag{52a, b}$$

where the asymptotic long-time value (supremum) of u is given by (41*a*, *b*). Figure 5(*a*, *b*) presents the respective dimensionless quantities

$$k_E = E^{\infty}/U_{esc}^2, \quad k_M = M^{\infty}/U_{esc}. \tag{53a, b}$$

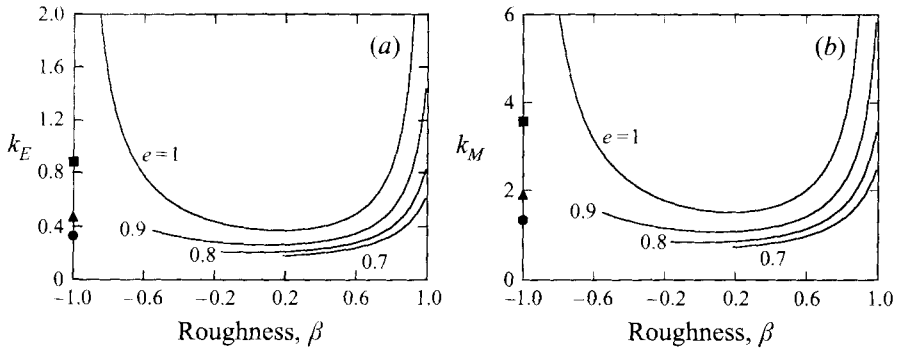

FIGURE 5. Ultimate escape energy and momentum *vs.* particles roughness: (*a*) normalized energy k_E; (*b*) normalized momentum k_M. Data for $\beta = -1$: ■, $e = 0.9$; ▲, $e = 0.8$; ●, $e = 0.7$.

The upper curves, obtained for elastic particles ($e = 1$) show that $k_M, k_E \to \infty$ at two extremes $\beta \to \pm 1$, corresponding to the conservative gas. In these cases the layer retrieves infinite kinetic energy, i.e. all particles are ultimately involved in the expansion process with the same velocity U_{esc}. Particle roughness induces kinetic energy losses, thereby yielding finite values of k_E, k_M (of elastic particles), which reach their minima at about $\beta = 0.2$.

The curves shown in figure 5(*a*, *b*) for inelastic particles ($e < 1$) exhibit the contribution of restitution coefficient to the overall kinetic energy losses, which combine with those stemming from the roughness to yield still lower values of k_M, k_E. These curves are plotted within the validity range of the hydrodynamic solution (Part 1), i.e. terminate at minimal β calculated for the respective restitution coefficient e.

For smooth particles ($\beta = -1$) one can obtain the following explicit analytical expressions for E^∞, M^∞:

$$E^\infty = 1.38326/\delta, \quad M^\infty = 1.87113/\delta, \tag{54a, b}$$

where δ (for smooth particles) reduces to

$$\delta = (4\pi/15)^{1/2}(1-e^2). \tag{55}$$

In figure 5(*a*, *b*) k_M, k_E calculated with these expressions are shown as single points. One can see that the smooth particles attain a larger ultimate kinetic energy than their counterparts, characterized by intermediate roughness $\beta \sim 0$, where the losses are maximal. One should note, however, that the kinetic energy (54*a*) and momentum (54*b*) are less than those obtained for absolutely rough particles. This may also be seen in figure 6, comparing the escape energy E^∞ for the two extremal cases $\beta = \pm 1$. Rough particles have more active internal degrees of freedom (rotational and translational) than smooth particles, characterized only by translational modes. Therefore, the relative amount of kinetic energy lost by the smooth particles is larger, which leads to smaller E^∞.

Having obtained the ultimate escape values of momentum M^∞ and energy E^∞ of the freely expanding layer, one can calculate the effective dimensionless mass of the escaping part:†

$$h_m = (M^\infty)^2/2E^\infty. \tag{56}$$

† Strictly speaking, the total escaping mass is infinite, since all particles (for all h) will ultimately gain a certain hydrodynamic velocity. However, for granules, characterized by large h this velocity is very small (decays exponentially with h). Therefore (52*a*, *b*) may be used to define an effective mass, which escapes with velocity $2E^\infty/M^\infty$.

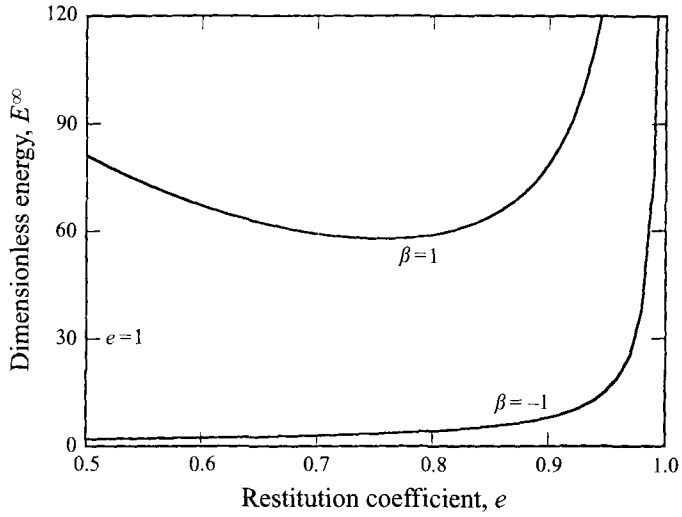

FIGURE 6. Ultimate escape energy E^∞ *vs.* particle restitution coefficient.

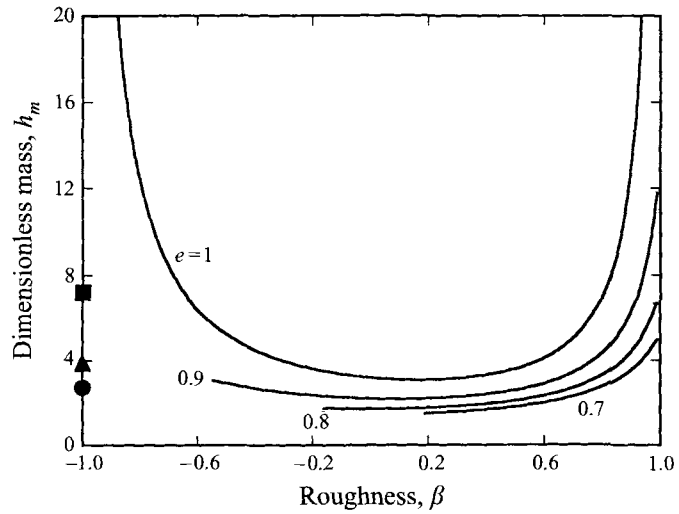

FIGURE 7. Ultimate effective escape mass h_m *vs.* particle roughness. Data for $\beta = -1$: ■, $e = 0.9$; ▲, $e = 0.8$; ●, $e = 0.7$.

This corresponds to the number of (packed) monolayers which effectively escape as a result of the expansion process. The corresponding dimensional mass is expressed by $h_m m/\sigma^2$. Figure 7 presents h_m *vs.* particle roughness for several values of e. Clearly, the curve calculated for $e = 1$ tends to infinity for $|\beta| \to 1$, because in these limits the kinetic energy losses vanish. This curve and others for $e < 1$ (plotted in the domain of existence of the solution) have minima, corresponding to maximal losses at about $\beta = 0.2$. Observe that h_m is independent of the initial granular temperature and determined only by the particle collisional properties. Specifically, for $e = 0.9$ about six monolayers of smooth particles and twelve monolayers of rough particles will escape. This agrees with the well known fact, reported in many studies, that no more than about six monolayers can be fluidized by vibrations (see, for example, Bachmann 1940; Kroll 1954; Gutman 1976; Clement & Rajchenbach 1991). In contrast, in Part 2 we succeeded in achieving fluidization of thicker layers, through a specific choice of the vibrational parameters.

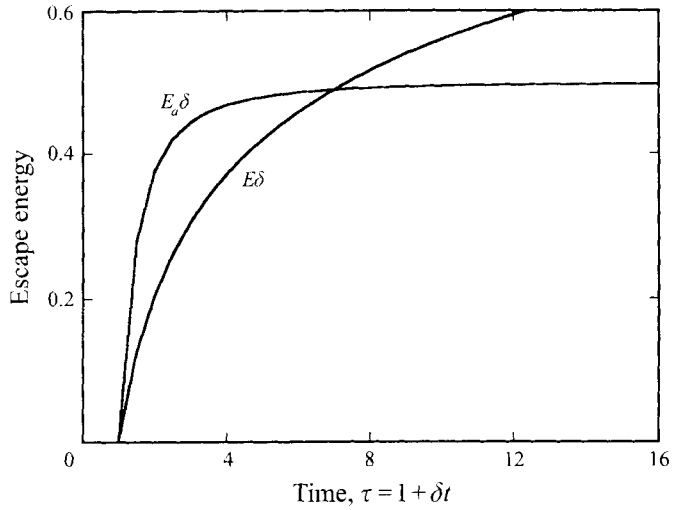

FIGURE 8. Dependence of escape energy of a granular gas of smooth particles on dimensionless time. E, exact solution (60); E_a, approximate solution (58).

We wish to use the solution obtained above to quantitatively assess the validity of the approximate model developed in Part 2 for vibrated granular layers of smooth particles. According to that model the effect of the expansion wave is to instantaneously transform all the kinetic energy of the granular random motion at the wave head into the escape energy of purely translational motion: $u_s = U_{esc} = O(E_{esc}(h))^{1/2}$. Using this assumption in the present circumstances of dilute gas, boundary conditions (22c) and definitions (20a, b), one obtains

$$E_{esc} = \exp(-2h\delta). \tag{57}$$

Now one can calculate the total layer escape energy by integrating (57) over the disturbed region:

$$E_a(t) = \int_0^{H(t)} E_{esc}(h)\,\mathrm{d}h = \frac{1}{2\delta}(1-\tau^{-2}), \tag{58}$$

where the wave head location $H(t)$ is related to τ via (12).

The exact value of $E(t)$ may be explicitly calculated from (42) in the form

$$E(t) = \frac{m\tilde{a}_0^2}{2\tilde{E}_0}\int_0^{H(t)} [u_s(\tau, h\delta)]^2\,\mathrm{d}h. \tag{59}$$

For smooth particles this equation can be rewritten using $\tilde{E}_0 = 0.9m\tilde{a}_0^2$ (see definitions (7) and using $\gamma = 5/3$) in the following form:

$$E(\tau) = \frac{5}{9\delta}\int_0^{\ln\tau} [u_s(\tau, x)]^2\,\mathrm{d}x. \tag{60}$$

Values of $E_a\delta$ and $E\delta$, respectively calculated from (58) and (60), are plotted in figure 8. For small times $\tau < 7$, E_a exceeds E, with the reverse trend prevailing at larger times. This is explained by noting that at large times the escaping particles progressively accelerate (at $e = 1$ up to a velocity of about three times the speed of sound), as a result of the pressure continously exerted by the 'deeper' particles. This energy transfer mechanism is not accounted for in the simplified model of Part 2. At large times this

model yields the escape velocity and, hence, E_a less than E. For large τ the effect of the above energy transfer mechanism is to cause a significant difference between E_a and E. Explicitly, at $\tau \to \infty$, $E^\infty = 3.07 E_a^\infty$.

At the wave head the present solution gives $u_s = 0$, whereas the model of Part 2 yields $u_s = U_{esc} = O(E_{esc})^{1/2}$. Since for small times, i.e. $\tau < 7$, all of the disturbed region is close to the wave head, the total contribution of the latter velocities results in $E_a > E$.

One can see, that for smooth particles, the difference $\Delta E = E_a - E$ depends on the dimensionless time t (see (7e)) and particle restitution coefficient, which is embodied in δ, given by (55). The e-dependence of ΔE is represented by the expression

$$f(\delta t)/\delta = f(\delta t)/0.915\,(1-e^2),$$

where $f = (E_a - E)\,\delta$ is the difference between the curves plotted in figure 8. For highly elastic particles $(1-e \ll 1)\,f$ is very small (of order $1-e^2$), hence $\Delta E = O(1)$. On the other hand, for inelastic particles $f = O(1)$ and $E_a - E \sim 1/\delta$. Therefore, for all e and t, $\Delta E = O(1)$.

One can, thus, conclude that calculation of the escape energy using the assumption of instant conversion of the granular temperature into E_a gives the right order of magnitude of that quantity, at least in the present model of a dilute granular gas. However, vibrated granular regimes considered in Part 2, were characterized by dense layers. Noting that for such layers kinetic energy losses are higher than in dilute gases, one can expect that for dense granular systems ΔE is less than the above estimation.

The above considerations are also applicable to estimation of the mass of the escaping part of the layer. Indeed, for dilute systems this mass will be larger because they dissipate less granular kinetic energy. Therefore the values of the escaping granular energy, mass (and momentum) serve as upper bounds on the values which would prevail for denser granular systems.

5. Discussion

In this paper closed-form analytical solutions for the t- and h-distributions of the hydrodynamic velocity, granular pressure and temperature of an expanding granular layer are obtained. This solution enables evaluation of the effects of particle kinetic energy losses, as embodied within their collisional properties, on u, P and ρ. In the absence of these losses ($e = 1$ and $|\beta| = 1$) our results reproduce the well-known self-similar solution for a conservative (molecular) gas. The effect of kinetic energy losses is to yield finite values of the energy E^∞ and momentum M^∞ gained by the freely expanding part of the layer.

Solution of the problem of the expansion of a granular gas into a vacuum may be generalized to the case of moderate or high initial particle density $\tilde{\rho}_0$. The physical ideas underlying three asymptotic expansions, developed in §3, can also be applied to dense granular systems. This will require specification of a more general equation of state and the concomitant expression for the sink term (Part 3). In all cases, however, the functional dependences of the kinetic energy sink term and the granular pressure upon the granular energy are the same as those given by (4) and (3), respectively. All such solutions have one important common feature, namely that the ultimate escape energy E^∞ of the infinite granular layer remains finite.

Both the compression wave (Part 3) and expansion wave solutions have shown that the maximal possible fluidized mass constitutes about 6–12 particle monolayers. The exact amount of fluidized granules is controlled by the rate of kinetic energy

dissipation, which is determined by the particle collisional properties. These results were obtained for the circumstances where no wave interactions occur. This apparently corresponds to the vibrational regimes characterized by large frequencies and small amplitudes, where only a limited amount of kinetic energy may be pumped into the granular layer.

The above finite values of the fluidized granular mass were obtained (both in Part 3 and in this study) on the basis of a model which does not account for gravitation. In fact, the role of the gravitational force in vibrofluidization of vertical granular layers is to bring the granules in contact with the bottom of the vibrating vessel. This factor is neither always efficient nor controlling the vibrofluidized state. Indeed, in order to achieve granular agitation one needs to increase the intensity (acceleration) of the vibrating vessel (Chlenov & Mikhailov 1972; Gutman 1968; Roberts 1984). However, with increasing acceleration the period of contact with the bottom (during which the kinetic energy is supplied) decreases: the layer meets the bottom once per several vibrational cycles. This means that the layer spends most of the time in the free flight, during which most (if not all) the kinetic energy is lost by dissipation. From this point of view more efficient vibrofluidization may be achieved by vibrational equipment (vibro-mills and vibro-mixers) with closed vessels, where the vibrated material impacts both with the top and the bottom of the working canister. In these cases the frequency of impacts is controlled by the amount of material in the canister and the vibrational regime chosen. For the high acceleration regimes (above $10\,g$) typical for this equipment, the effect of the gravity force on the vibrational motion is small.

In fact, vibrofluidization may even be achieved without gravity, i.e. in outer space. Other space-related applications of the wave propagation processes in granular materials will be considered in separate studies.

The relatively small escaping mass (6–12 granular monolayers) may raise a question about validity of the hydrodynamic continuum model. One should note, however, that the extension of the physical granular system in a collisional state is larger because the average distance between the granules may well exceed their diameter, especially for the dilute granular gas considered here. Additionally, one may be encouraged by the agreement between the above estimate and the fluidized portion of the granular layer observed in several experimental studies (Bachmann 1940; Clement & Rajchenbach 1991). An unequivocal conclusion about the applicability of the hydrodynamic solution to systems including such a small amount of particles can only be drawn on the basis of comparison with the results of particle dynamic simulations. Unlike the complicated simulation of real physical or industrial systems, the rigorous solutions of the model problems obtained here and in Part 3 may provide a basis for such a comparison.

The hydrodynamic solutions obtained in this paper and in Part 3 may be used to verify the accuracy of PDS and to choose the necessary amount of particles to be included in the system. On the other hand, a comparison between the continuum and PDS solutions is useful for delineating the applicability limits of the former methods in cases where the existence of the hydrodynamic solution is questionable. Moreover, the exact hydrodynamic solutions constitute important milestones necessary for development and verification of computational techniques, aimed at describing physical experiments or industrial processes involving granular materials.

The authors gratefully acknowledge partial financial support of the Basic Research Foundation administrated by the Israel Academy of Sciences. A. G. acknowledges the support of the Gileadi Program.

REFERENCES

AHMAD, K. & SMALLEY, I. J. 1973 Observation of particle segregation in vibrated granular systems. *Powder Technol.* **8**, 69–75.

BACHMANN, D. 1940 Bewegungsvorgänge in schwingmühlen mit trockner mahlkörperfüllung. *Verfahrenstechnik Z. VDI-Beiheft* **2**, 43–55.

CHLENOV, V. A. & MIKHAILOV, N. D. 1972 *Vibrofluidized Beds.* Moscow: Nauka (in Russian).

CLEMENT, E. & RAJCHENBACH, J. 1991 Fluidization of a bidimensional powder. *Europhys. Lett.* **16**, 133–138.

COURANT, R. & FRIEDRICHS, K. O. 1948 *Supersonic Flow and Shock Waves.* Interscience.

GOLDSHTEIN, A. & SHAPIRO, M. 1995 Mechanics of collisional motion of granular materials. Part 1. General hydrodynamic equations. *J. Fluid Mech.* **282**, 75–114.

GOLDSHTEIN, A., SHAPIRO, M. & GUTFINGER, C. 1996 Mechanics of collisional motion of granular materials. Part 3. Self-similar shock-wave motion. *J. Fluid Mech.* **316**, 29–51.

GOLDSHTEIN, A., SHAPIRO, M., MOLDAVSKY, L. & FICHMAN, M. 1995*a* Mechanics of collisional motion of granular materials. Part 2. Wave propagation through a granular layer. *J. Fluid Mech.* **95**, 349–382.

GOLDSHTEIN, A., SHAPIRO, M., MOLDAVSKY, L. & FICHMAN, M. 1995*b* Wave propagation as mixing mechanisms in vibrated layers of solid granules. *Proc. First Israel Conference on Conveying and Handling of Bulk Solid Materials, Herzlia, May 1995.*

GUTMAN, I. 1968 *Industrial Uses of Mechanical Vibrations.* London: Business Books.

GUTMAN, R. G. 1976 Vibrated beds of powders. Part I: A theoretical model for the vibrated bed. *Trans. Inst. Chem. Engrs* **54**, 174–183.

JENKINS, J. T. & RICHMAN, M. W. 1985 Kinetic theory for plane flows of a dense gas of identical, rough, inelastic, circular disks. *Phys. Fluids* **28**, 3485–3494.

JENKINS, J. T. & RICHMAN, M. W. 1988 Plane simple shear of inelastic circular disks: the anisotropy of the second moment in the dilute and dense limits. *J. Fluid Mech.* **192**, 318–328.

KROLL, W. 1954 Über das Verhalten von Schüttgut in Lotrecht Schwingenden Gefäben. *Forsch. Geb. Ingenieur* **20**, 2–15.

LAN, Y. & ROSATO, A. D. 1995 Macroscopic behavior of vibrating beds of smooth inelastic spheres. *Phys. Fluids* **7**, 1818–1831.

LUDING, S., CLEMENT, E., BLUMEN, A., RAJCHENBACH, J. & DURAN, J. 1994*a* Studies of column of beads under external vibrations. *Phys. Rev.* E **49**, 1634–1646.

LUDING, S., HERRMANN, H. J. & BLUMEN, A. 1994*b* Simulations of two-dimensional arrays of beads under external vibrations: Scaling behavior. *Phys. Rev.* E **50**, 3100–3108.

LUN, C. K. K. 1991 Kinetic theory for granular flow of dense, slightly inelastic, slightly rough spheres. *J. Fluid Mech.* **233**, 539–559.

LUN, C. K. K. & BENT, A. A. 1994 Numerical simulation of inelastic, frictional spheres in simple shear flow. *J. Fluid Mech.* **258**, 335–353.

LUN, C. K. K. & SAVAGE, S. B. 1987 A simple kinetic theory for granular flow of rough, inelastic, spherical particles. *Trans. ASME J. Appl. Mech.* **54**, 47–53.

MOODY, D. M. 1990 Unsteady expansion of an ideal gas into a vacuum. *J. Fluid Mech.* **214**, 455–468.

RASKIN, KH. I. 1975 Application of the methods of physical kinetics to problems of vibrated granular media. *Dokl. Acad. Nauk SSSR* **220**, 54–57.

RICHMAN, M. W. 1989 The source of second moment of dilute granular flows of highly inelastic spheres. *J. Rheol.* **33**, 1293–1306.

ROBERTS, A. W. 1984 *Handbook of Powder Science and Technology.* Van Nostrand Reinhold.

SAVAGE, S. B. 1988 Streaming motions in a bed of vibrationally fluidized dry granular material. *J. Fluid Mech.* **194**, 457–478.

SAVAGE, S. B. 1992 Instability of unbounded uniform granular shear flow. *J. Fluid Mech.* **241**, 109–123.

VAN DYKE, M. D. 1968 *Perturbation Methods in Fluid Mechanics.* Academic Press.

ZHANG, Y. & CAMPBELL, C. 1992 The interface between fluid-like and solid-like behaviour in two-dimensional granular flows. *J. Fluid Mech.* **237**, 541–568.